

## Saltating particles over flat beds

By PHILIP NALPANIS<sup>1</sup>†, J. C. R. HUNT<sup>2</sup>‡  
AND C. F. BARRETT<sup>3</sup>||

<sup>1</sup>Department of Engineering, University of Cambridge, Trumpington Street,  
Cambridge CB2 1PZ, UK

<sup>2</sup>Department of Applied Mathematics & Theoretical Physics, University of Cambridge,  
Silver Street, Cambridge CB3 9EW, UK

<sup>3</sup>Department of Trade and Industry, Warren Spring Laboratory, Stevenage,  
Herts SG1 2BX, UK

(Received 5 February 1988 and in revised form 2 December 1992)

Measurements of ejection and impact velocities, trajectory lengths and maximum rise heights of sand grains (median diameters 118 and 188  $\mu\text{m}$ ) in saltation over a flat sand bed in a wind tunnel have been obtained from the digitization of multiple-image photographs. The mean angle of ejection is found to be about  $30^\circ$  from the horizontal (rather than  $90^\circ$ ) with mean vertical ejection velocity of about  $2u_*$ , where  $u_*$  is the friction velocity.

Trajectories of saltating grains have been computed, using the measurements of the initial ejection velocities and the mean velocity profile of the air flow. The results largely agree with our measurements, and those of others, of mean values of maximum rise height, and the angles and velocities of particles at impact with the bed, including measurements of saltating snow particles. The velocity results are correlated with  $u_*$ , the friction velocity.

An essential point is that, even for particles as small as 100  $\mu\text{m}$ , the fact that the drag law is nonlinear (i.e. non-Stokesian) means that the large horizontal mean velocity acts to increase the vertical component of drag on particles. This effect reduces the height to which they rise by 40% to 50% compared with the value in still air for a given vertical ejection velocity.

Using the measured probability distribution of ejection velocities, an ensemble of trajectories was computed and thence the average horizontal velocity  $\langle v_1 \rangle$  of particles at a given height and the vertical profiles of streamwise fluxes  $f_1(z)$  and concentrations of sand grains over a flat bed. It was found that above the threshold wind speed  $f_1(z) \propto \exp(-\lambda gz/u_*^2)$ , where the coefficient  $\lambda$  varies over about 50%. The rapid increase in  $\langle v_1 \rangle$  above the mean height of the particles, and the exponential decrease with height of the computed flux profile both agree with several sets of measurements in wind tunnels and in the field (collated here for the first time). However, unanswered questions about saltation still remain.

A model equation is proposed connecting the integrated horizontal flux  $F_1(z) = \int_0^\infty f_1(z) dz$ , the vertical upwards flux  $f_{3E}$  and the average length  $l$  of trajectories. This suggests a significant correlation between  $l$  and  $f_{3E}$ .

---

† Now at DNV Technica Ltd, Lynton House, 7/12 Tavistock Square, London WC1H 9LT, UK.

‡ Now at Meteorological Office, Bracknell, Berks, RG12 2SZ, UK.

|| Home address: 2 Byron Close, Stevenage, Herts, SG2 0JE, UK.

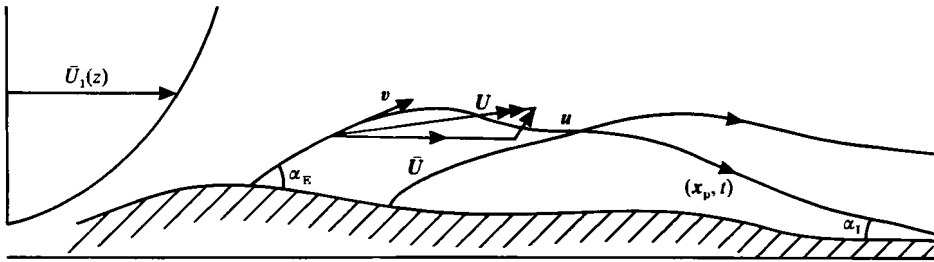


FIGURE 1. Definition sketch of sand grain velocity  $v$  in an air flow with mean velocity  $\bar{U}$ , fluctuating velocity  $u$  and total velocity  $U$ .

## 1. Introduction

The airborne movement of particles of sand, dust, soil and snow causes some of the major environmental problems of the world, ranging from the catastrophic, as in desertification, to the inconvenient as in dust blown from stockpiles or as snow drifts on roads (as discussed in the conference proceeding edited by Barndorff-Nielsen 1985). The primary model of transport of large particles (typically 40–600  $\mu\text{m}$ ) is by saltating or ‘jumping’ trajectories near the surface. Despite much research in the past (especially the pioneering research of Bagnold 1941 and the dynamical studies of Owen 1964), there remain many uncertainties about the mechanisms of particles leaving the surface, the velocities of the particles in their trajectories and how they relate to the velocities of the air flow, the statistics of the trajectories, and the relative importance of the different forces acting on the particles.

An excellent recent review on several possible mechanisms that exist for the raising (or entraining) of particles from a bed into an airflow (figure 1) has been written by Anderson, Sørensen & Willetts (1991). We have included here some additional references that were omitted in their review.

As the wind stress is increased, the extra drag on the particles caused by fluctuations in the wind speed, i.e. by turbulent eddies, becomes great enough to change their trajectories significantly from the elongated parabolas characteristic of saltation. Owen (1964) suggested that the criterion for this change should be based on whether the drag force on the particle by the turbulent eddies is greater or less than its weight, i.e.  $u_*^*/(ga\rho_p/\rho) > 1$  or  $< 1$ , where  $u_*$  is the friction velocity,  $\rho_p$  the density of the particle,  $\rho$  mean density,  $a$  particle radius and  $g$  is the acceleration due to gravity. Recent investigations of this aspect of wind-blown particles using computer simulations of their motion have been described by Hunt & Nalpanis (1986), Nalpanis (1985) and Anderson (1987).

The use of special wind tunnels designed for studies of dust and sand movement, techniques for recording and analysing particles in motion, and computers for calculating and analysing particle trajectories, has led to new insights into the mechanics of the saltation process and, at higher wind speeds, the transition to suspension. In this paper we concentrate on saltation. Other research groups have also measured and computed complete trajectories or only certain features of trajectories, such as ejection angles (e.g. White & Schulz 1977; Sørensen 1985; Araoka & Maeno 1981; Willetts & Rice 1985). The main contribution of this study is to use measurements of the distribution of velocities of particles leaving the surface in conjunction with the computed trajectories to predict the vertical profiles of horizontal flux and of average particle velocities.

The predictions are compared with our own recent wind-tunnel measurements of

sand fluxes at Warren Spring Laboratory and those of Gillette & Stockton (1986), with laboratory shear measurements by Maeno *et al.* (1979), with field measurements of sand flux profiles by Rasmussen, Sørensen & Willetts (1985), and with mean velocity measurements by Greeley, Williams & Marshall (1983).

The research was carried out as part of an industrially sponsored project on 'Suspension, Transport and Deposition of Dust from Stockpiles', carried out at the University of Cambridge and at Warren Spring Laboratory (UK Department of Trade and Industry). Stockpiles may be defined as open-air storage piles of mineral material (e.g. coal, ores, limestone). The aims of the work described in this paper were, firstly, to understand and describe quantitatively the initial motion of solid particles leaving a surface; secondly, to model their motion in turbulent shear flow. The model has been combined with models for flow over stockpiles (developed from a combination of theoretical and experimental work) to predict the dispersion of dust from stockpiles (Nalpanis & Hunt 1986). Clearly, such understanding and models may also be applied to many other problems such as aeolian transport of sand, soil and snow.

## 2. Our experiments

The wind-tunnel used in our experiments at Warren Spring Laboratory was of the open-circuit type, with a working section 5 m long, 1.2 m wide and 0.6 m high (figure 2). The fan was upwind of the tunnel contraction; downwind of the diffuser there were filters to trap any sand grains still airborne. A 20 cm deep logarithmic profile was generated by Counihan's (1969) technique of a 0.09 m fence and vorticity generators; a flat board 1.25 m long was placed immediately downwind of the vorticity generators because the disturbed flow in this region was found to lead to irregular initiation of saltation of sand. Downwind of the board the floor was covered with loose sand to a depth of 0.02 m, with its surface at the same height as the board, with containing walls round it another 0.02 m higher. Prior to each run fresh sand was applied to the surface, which was then smoothed off.

Dry builders' sand was used, with a density of  $2650 \text{ kg m}^{-3}$ . Two size ranges were used, with median diameters respectively of 118 and 188  $\mu\text{m}$ . Their size distributions are shown in figure 3: they are log-normal with geometric standard deviations of 1.17 and 1.18 respectively.

Profiles of mass flux and wind speed were determined at distances of 2, 4 and 6 m from the upwind edge of the sand bed. Only a small change was found from the values at 2 m and none between 4 and 6 m. The measurements used were made at 6 m. Details of the profiles are reported by Barrett & Upton (1988).

The mean wind profile  $\bar{U}_1(z)$  was measured over the sand bed both when the threshold wind speed was less than the threshold value to initiate saltation and when the wind speed was great enough for saltation to occur (figure 2*b*).  $\bar{U}_1(z)$  was found to be a linear function of  $\log z$  in both cases. From the slope of the log-linear plot the magnitude of the friction velocity  $u_*$  was calculated (figure 2*b*). No zero-plane displacement was used. When  $u_*$  was significantly greater than the threshold value  $u_T$ , the roughness length  $z_0$  was found to be about 100  $\mu\text{m}$ . For  $u_* < u_T$  the surface was effectively hydraulically smooth. This change of  $z_0$  is consistent with the observation that there was a slight departure of  $\bar{U}_1(z)$  from the log profile within the saltating layers of particles. The profile  $\bar{U}_1(z)$  was certainly neither constant nor linear with height within this layer (Owen 1964), perhaps because the wind speed was only about 60% above its threshold. (See also Raupach 1991.) Other investigators have also found small changes in these conditions, as in the field experiments of Rasmussen *et al.*

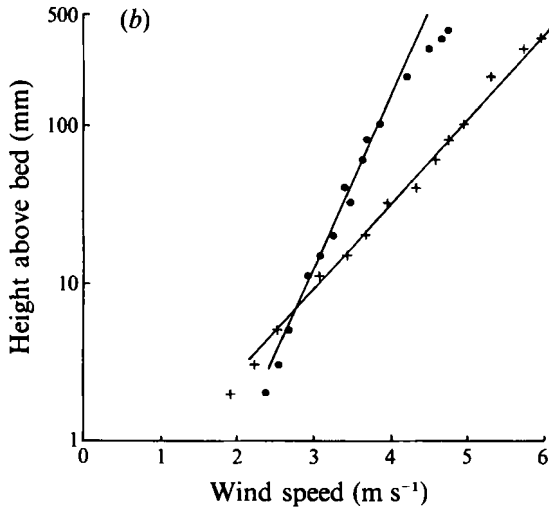
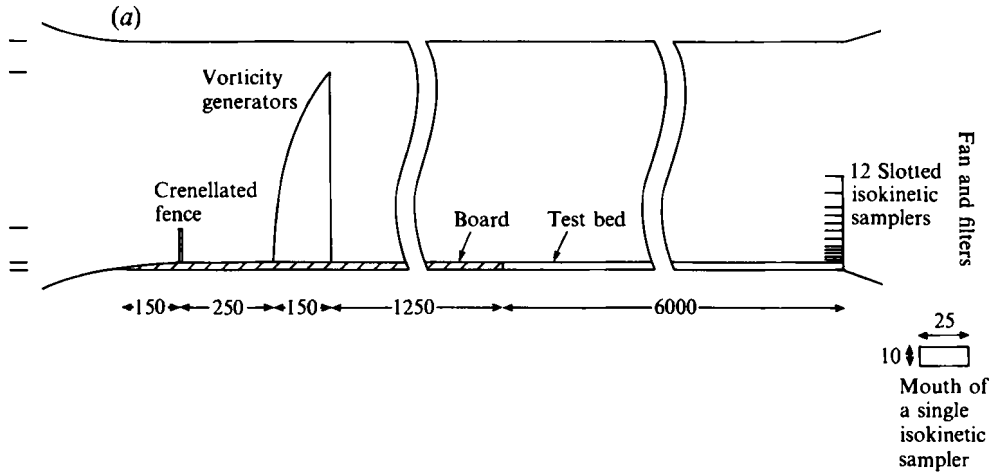


FIGURE 2. Warren Spring wind tunnel for sand movement: (a) working section showing the 'Counihan' boundary-layer thickening devices and the isokinetic samplers (dimensions in mm); (b) mean velocity profiles over the sand bed, ●,  $u_* = 0.17 \text{ m s}^{-1}$  (below threshold); +,  $u_* = 0.34 \text{ m s}^{-1}$  (above threshold).

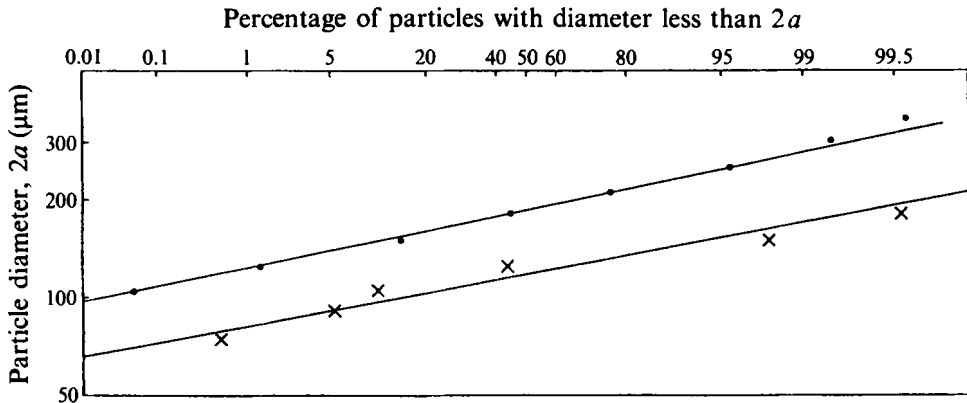


FIGURE 3. Size distribution of sands used in saltation experiments: ●, median diameter 188  $\mu\text{m}$ ; +, median diameter 118  $\mu\text{m}$ .

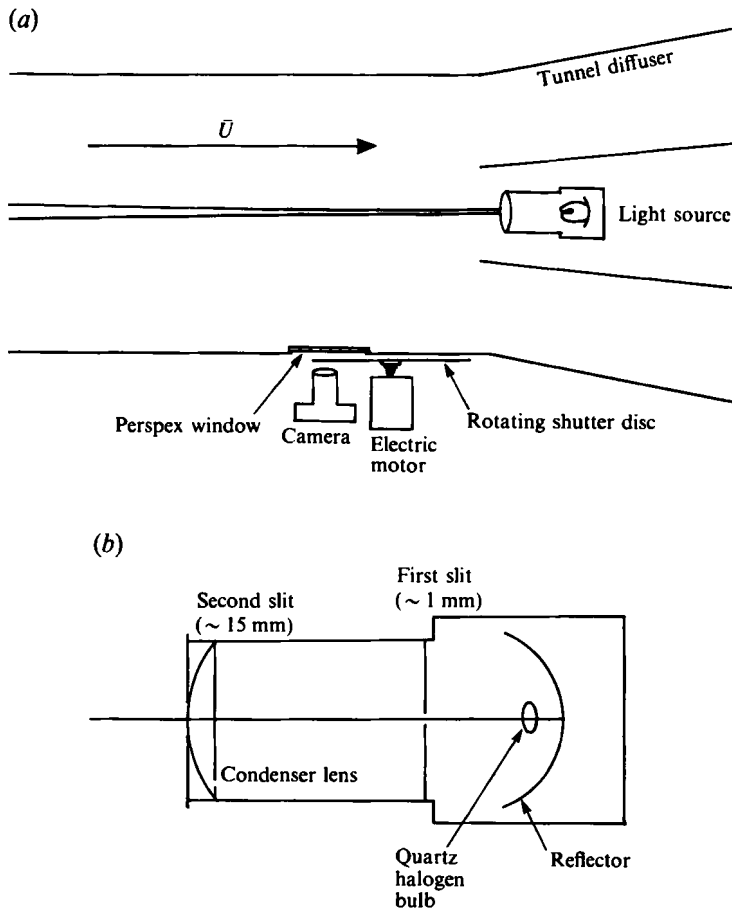


FIGURE 4. Lighting arrangement for photographing sand particle trajectories: (a) layout of source, camera and rotating shutter; (b) detail of light source.

(1985). During the experiments the tunnel reference speed was measured with a vane anemometer situated on the tunnel centreline, immediately above the region being observed. The depth of the tunnel, 0.6 m, was sufficiently large compared with the boundary-layer depth of about 0.14 m and the layer of saltating particles (0.02 m) that there was little acceleration of the flow outside the boundary layer and therefore a negligible pressure gradient along the tunnel. Shallower tunnels have led to serious errors in  $u_*$  and incorrect interpretations (for reasons explained by Owen & Gillette 1985).

The threshold values were determined by finding the maximum velocity that gave a zero saltation flux. For the sand used here, we found that the threshold value of  $u_*$ ,  $u_T$ , was about  $0.18 \text{ m s}^{-1}$  for the  $188 \mu\text{m}$  grains and  $0.16 \text{ m s}^{-1}$  for the  $118 \mu\text{m}$  grains. These values were about 10% below the minimum value given by the formulae of Fletcher (1976) and Iverson & White (1982).

Flux profiles of particles in saltation were measured by a vertical array of traps. The sand was accumulated in 'isokinetic' samplers, whose inlet speeds were adjusted to the local velocity profile, in order to avoid errors found in the use of simple slot traps in measuring the fluxes of small particles at low wind speeds (e.g. Bagnold 1941; White 1982).

Saltation trajectories of sand grains were measured by multiple-image photography (by a technique similar to that Araoka & Maeno 1981 used for snow particles). We chose this method in preference to high-speed ciné because it is possible thereby to see the whole or a substantial part of a trajectory. It is easier to follow each trajectory from one point to the next (especially where several trajectories cross or run close together) and thus easier to digitize it. The disadvantage is that it is difficult to see what happens when a saltating particle impacts onto the surface, and to study the impact-ejection process.

In order that photographs should not contain too many particle trajectories (for measurement) and so that the camera could be focused on the particles, the illumination source was designed to provide a thin vertical 'strip' of light straight along the centre of the tunnel. Its vertical depth was sufficient to reach from the surface up to at least the maximum height expected for particle trajectories. Figure 4(a) shows the 1 kW quartz-halogen light in the diffuser shining directly upwind through a series of slits and a condenser lens (as shown in figure 4b) which gave a concentrated beam about 1 cm wide in the observation region.

To interrupt the light, a rotating shutter was placed between the camera lens and the tunnel window (so that the light entering the camera was interrupted rather than the light source itself). This consisted of a stiff black card disc with eight holes of similar dimensions to the lens, mounted on an electric motor rotating at about 3000 r.p.m.; holes and solid portions of the disc subtend the same angle. The effect of this was to divide each trajectory into light and dark segments of known time duration of about 2.3 ms (the rotation speed was measured using a hand-held optical tachometer with a resolution of 20 r.p.m.). We found experimentally that this gave segments short enough for rapid changes in velocity to be resolved. At the wind speeds used (approx.  $4 \text{ m s}^{-1}$ ) typical trajectories are about 0.04 s long; the camera shutter was therefore opened for (typically)  $\frac{1}{15}$  s in order to record a reasonable number of near-complete trajectories. A typical photograph taken by this method is shown in figure 5.

The camera used was a 35 mm Nikon FE camera with an 85 mm telephoto lens, mounted on a tripod. The film was Ilford XP1 rated at 1600 ASA. The camera was fitted with an automatic winder and electrically operated shutter release.

In order to prevent stray light reaching the camera, several precautions were taken. The rails inside the tunnel (capping the sand bed retaining walls) were covered with black flock-paper where they could be seen by the camera. A large black canopy was placed outside the tunnel around the camera to keep out direct external light.

The particle trajectories were digitized by using a film measuring machine in the Cambridge University Engineering Department. The negatives were analysed directly, being enlarged by the machine to appear on a TV monitor, whose resolution appears to be better than film grain size (magnification about  $250\times$ ). The data were recorded on a punched paper-tape and transferred to the University's computer (IBM 3081) for calculation of velocities and other quantities.

The computer analysis was as follows: (i) transform measured coordinates to real distances; (ii) calculate horizontal and vertical velocities ( $v_1, v_3$ ); (iii) smooth (separately) velocity components; (iv) extrapolate each measured trajectory to the surface by computing the trajectory back to the surface; (v) collect trajectory statistics.

Step (iv) was carried out in order to determine ejection ( $v_{1E}, v_{3E}$ ) and impact velocities ( $v_{1I}, v_{3I}$ ), trajectory heights ( $h$ ) and lengths ( $l$ ), because the initial and final stages of trajectories were frequently not visible on photographs. The angles of ejection  $\alpha_E$  and impact  $\alpha_I$  were measured for each trajectory. Their average values  $\langle \alpha_E \rangle$  and  $\langle \alpha_I \rangle$  were calculated. This value exceeded the angle derived from the ratio of the

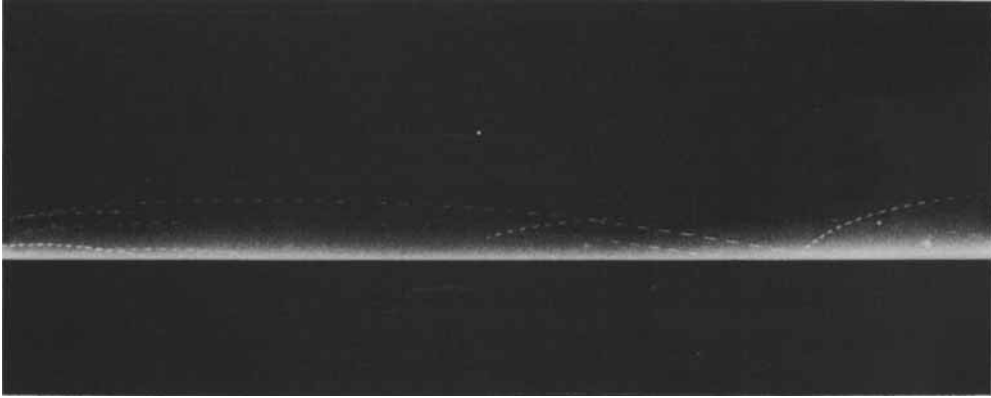


FIGURE 5. Trajectory photographs for 188  $\mu\text{m}$  median diameter particles with an interrupted light source.  $\bar{U}_{\text{ref}} = 3.8 \text{ m s}^{-1}$ .

average vertical and horizontal velocities of ejecting particles  $\langle v_{3E} \rangle / \langle v_{1E} \rangle$  which we define as  $\tan \langle \alpha_E \rangle^*$  (table 1). The ejection speed  $v_E$  is taken to be given by  $v_E^2 = v_{1E}^2 + v_{3E}^2$ , because lateral ejection velocities  $v_{2E}$  are assumed to be small.

In transforming coordinates to real distances, three processes were involved, namely scaling, correcting for tilt, and establishing distance above the surface. The first was accomplished using a scale photograph taken at the beginning of each run. For the second problem we examined the sand, which produces a dark (on the negatives) strip of finite width (visible as a light strip in figure 5). The true orientation of this strip is taken to be horizontal, and its apparent tilt (due either to camera tilt or to placing of negatives on film measuring table) calculated. Since the strip was of finite width on the negatives and represents the width of the light, it is impossible to tell whether particle trajectories are over the middle or edge of the strip, and hence where the correct datum is for any particular trajectory. We assumed that it was central because it was equally likely to be either side of this and therefore the calculated statistical distributions of trajectory parameters was not appreciably affected by this assumption (though the individual heights may be up to 1.2 mm out).

For a time interval  $\Delta t$  and particle position coordinates  $y_1, y_3$ , the velocities at the  $i$ th point were simply taken to be

$$v_1^i = \frac{y_1^{i+1} - y_1^{i-1}}{2\Delta t} \quad \text{and} \quad v_3^i = \frac{y_3^{i+1} - y_3^{i-1}}{2\Delta t}.$$

Smoothing was done using a cubic spline, which by comparing smoothed and simulated trajectory velocity plots against time was found to give better results than a power series. Even so, a significant number of trajectories did not give a satisfactory fit and were rejected: only those trajectories which were smooth and fitted the spline, and also conformed approximately to the computed trajectory were used. Furthermore, only trajectories which had upward-bound portions were extrapolated back to their ejection point, and only those with downward-bound portions were extrapolated to impact: this was done to minimize the error in the extrapolation (which could be due to incorrect starting height or initial velocity). Extrapolation was carried out by time-stepping (forward or backward) the basic equation of motion given in (2) and (3) in §4, where the relative velocity is calculated from the particle speed and the measured mean wind profile which has the logarithmic form  $\bar{U}_1(z) = (u_*/k) \ln(z/z_0)$ . Since the 188 and 118  $\mu\text{m}$  particles have a terminal velocity appreciably greater than

| Experiment  | WR          |         | WS               | NHB            |         |         | AM     | Comp't'n              |                  |
|---|-------------|---------|------------------|----------------|---------|---------|--------|-----------------------|------------------|
| Material  | Quartz sand |         | Glass spheres    | Builders' sand |         |         | Snow   | Sand particles        |                  |
| Size ( $\mu\text{m}$ )                                    | 355-600     | 250-355 | 150-250          | 360-710        | 150-300 | 150-300 | 90-150 | 100                   | 200              |
| $u_*$ ( $\text{m s}^{-1}$ )                               | 0.39        | 0.39    | 0.39             | 0.96           | 0.205   | 0.20    | 0.18   | 0.30 <sup>†</sup>     | 0.4 $\leftarrow$ |
| $\langle v_E \rangle$ ( $\text{m s}^{-1}$ )               | 2.25        | 2.16    | 2.40             | 0.69           | 0.76    | 0.88    | 0.81   | 1.04                  | 1.0 $\leftarrow$ |
| $\langle \alpha_E \rangle$ (deg.)                         | 21.3        | 24.9    | 33.4             | 49.9           | 41.0    | 34.0    | 35.0   | 49                    | 45 $\leftarrow$  |
| $\langle \alpha_E \rangle^*$ (deg.)                       | —           | —       | —                | —              | —       | 23      | —      | 28                    | 45 $\leftarrow$  |
| $\langle v_1 \rangle$ ( $\text{m s}^{-1}$ )               | 3.60        | 3.50    | 3.94             | 1.60           | 1.50    | 1.40    | 1.30   | 1.9                   | 4.1              |
| $\langle \alpha_1 \rangle$ (deg.)                         | 12.7        | 11.7    | 9.6              | 13.9           | 14.0    | 13.0    | 11.0   | 11                    | 9                |
| $\langle \alpha_1 \rangle^*$ (deg.)                       | —           | —       | —                | —              | 13      | 13      | 11     | 13                    | 9                |
| $\langle h \rangle$ (mm)                                  | 48          | 64      | 56 <sup>v</sup>  | —              | 6.4     | 5.6     | 4.8    | 1.0-19.3 <sup>⊗</sup> | 29.4             |
| $\langle l \rangle$ (mm)                                  | 640         | 720     | 800 <sup>v</sup> | —              | 72      | 80      | 64     | 100 <sup>(M)</sup>    | 441              |
| $\langle v_E \rangle / u_*$                               | —           | —       | 5.8              | 1.8            | 3.8     | 4.3     | 4.6    | 3.3                   | 2.5 $\leftarrow$ |
| $\langle v_{3E} \rangle / u_*$                            | —           | —       | 2.1 <sup>φ</sup> | —              | 2.1     | 2.0     | 2.1    | 1.6                   | 1.8 $\leftarrow$ |
| $v_{31} / v_{3E}$   | 0.86        | 0.65    | 0.47             | 0.73           | 0.73    | 0.64    | 0.53   | 0.78                  | 0.66             |
| $\alpha_E / \alpha_1$                                     | 2.01        | 2.73    | 4.21             | 3.6            | 2.9     | 2.6     | 3.2    | 2.5                   | 5                |
| $\langle h \rangle / \frac{\langle v_{3E}^2 \rangle}{2g}$ | —           | —       | —                | —              | 0.56    | 0.53    | 0.59   | 0.52 $\pm$ 0.3        | 0.58             |
| $\langle h \rangle / \frac{\langle v_{3E} \rangle^2}{2g}$ | —           | —       | —                | —              | 0.71    | 0.65    | 0.69   | —                     | 0.58             |
| $\langle l \rangle / \frac{\langle v_{3E}^2 \rangle}{2g}$ | —           | —       | —                | —              | 6.3     | 7.9     | 7.4    | 7.0 <sup>(M)</sup>    | 8.8              |

$\leftarrow$  Input to computation.

$\phi$  Calculated from  $\langle v_E \rangle \sin \langle \alpha_E \rangle$ .

\* Defined by  $\tan^{-1}(\langle v_{3E} \rangle / \langle v_{1E} \rangle)$ .

† Estimate from their velocity profile.

⊗ A selection of five trajectories given by AM ( $u_{3E}$  measured for each trajectory).

$\pm$  A range of particular values.

<sup>v</sup> WR obtained these values by extrapolation.

(M) Maeno.

TABLE 1. Saltation experiments and computations. Names of experimenters: WR, Willetts & Rice (1985); WS, White & Schulz (1977); NHB, Nalpanis, Hunt & Barrett (1993 - this paper, for runs 01, 02, 03); AM, Araoka & Maeno (1981); (M) Maeno *et al.*

$u_*$ , they are not affected by turbulence and hence this extrapolation, which uses only the mean wind speed, is taken to be valid.

Several authors (e.g. Maeno *et al.* 1979; Rasmussen *et al.* 1985) have suggested that in saltation the wind speed close to the surface (in our case, within a few mm of it) is faster than that given by the logarithmic form above; perhaps even having a constant value below a certain height  $z_1$ .

To test the sensitivity of our trajectories to the wind profile we computed saltation trajectories by assuming that the mean velocity was constant below a height  $z_1$  (i.e.  $\bar{U}_1(z < z_1) = \bar{U}_1(z_1)$ ), rather than decreasing as in the logarithmic profile. We found no significant effect on the trajectories.

From the measurements of the velocities and dimensions of 377 saltation trajectories, in runs 01, 02, 03, distributions and mean values of various quantities were obtained. The mean values are presented in table 1, along with data from other experiments and computations of a typical trajectory. The experiments are discussed in §3 and the computations in §4.



### 3. Discussion of measurements of saltation velocities and trajectories

#### 3.1. Previous experiments

To compare our measurements with those from other laboratory experiments it is necessary to note a few important points about those experiments.

Willetts & Rice (1985, referred to as WR hereafter) have made the most detailed study hitherto of the impacting and ejection of saltating particles at the surface of the bed. They showed how when a particle impacts on a bed it collides with other particles on and below the surface of the bed and induces several particles to be ejected from the surface at a location, generally a few diameters downwind of the position of initial impact.

This picture has been confirmed by computer simulation of impacting particles by Anderson & Haff (1991). WR were less interested in photo-analysing trajectories above the bed than in the movement of particles at the surface of the sand bed, and recorded many trajectories that never rose into the field of view above the surface (as used in our analysis). Consequently their average values of the ejection and impact angles ( $\langle\alpha_E\rangle$ ,  $\langle\alpha_I\rangle$ ) should be smaller than our measured values and their average horizontal ejection velocity  $\langle v_{1E}\rangle$  should be larger. However, their values of the vertical ejection velocity  $\langle v_{3E}\rangle$  and the impact velocities (largely determined by movements well above the surface) should be similar to ours. Note that WR used three ranges of particle sizes, which are defined in table 1.

In White & Schulz's (1977, referred to as WS hereafter) experiments on saltation of glass spheres, with a specific gravity 2.5 and diameters ranging from 350 to 710  $\mu\text{m}$  in an airflow, the trajectories were measured photographically.

The experiments of Araoka & Maeno (1981, referred to as AM hereafter) were conducted in a wind tunnel (0.5  $\times$  0.5 m in cross-section) with snow laid down on the surface; snow was also introduced from a source near the top of the wind tunnel. Their experiments were conducted at  $-9^\circ\text{C}$ ! Their photographed trajectories look similar to ours, as shown in figure 5. In addition to take-off and impact statistics, and the heights and lengths of trajectories, they measured the horizontal and vertical velocities of the particles along their trajectories.

#### 3.2. Comparisons between measurements of trajectories

Our measurements of the mean ejection angles  $\langle\alpha_E\rangle$  were in the range  $34\text{--}41^\circ$ , with a standard deviation (obtained from figure 6) of about  $19^\circ \pm 2^\circ$ , i.e. half the mean. This value of  $\langle\alpha_E\rangle$  is considerably less than the value of  $90^\circ$  originally suggested by Bagnold (1941) and assumed by Owen (1964). It is less than the values of  $50^\circ$  measured by WS for their larger glass spheres and  $49^\circ$  measured by AM for 118  $\mu\text{m}$  snow particles, but greater than the range  $21\text{--}33^\circ$  measured by WR. This lower value was explained in §3.1. Our results are within one standard deviation of all these other measurements.

Note that if the ejection angle is estimated from the mean ejection vertical and horizontal velocity components, and defined as  $\langle\alpha_E\rangle^*(=\tan^{-1}(\langle v_{3E}\rangle/\langle v_{1E}\rangle))$ , it is found to be only about  $23^\circ$ . This means that in a small proportion of the ejections  $v_{3E}$  is large and  $v_{1E}$  is small, as can be seen on photographs, and the histogram of  $\alpha_E$  in figure 6.

Our average resultant ejection speeds  $\langle v_E\rangle$  were  $3.5u_*$  and  $4.4u_*$  compared with  $1.8u_*$ ,  $3.3u_*$  and  $5.8u_*$  for WS, AM and WR respectively. The standard deviation in  $v_E$  was about  $2u_*$ . However, the fact that WS's larger particles had a lower value of  $v_E$  (and a higher  $\alpha_E$ ) is explicable if they missed many trajectories close to the surface. Our

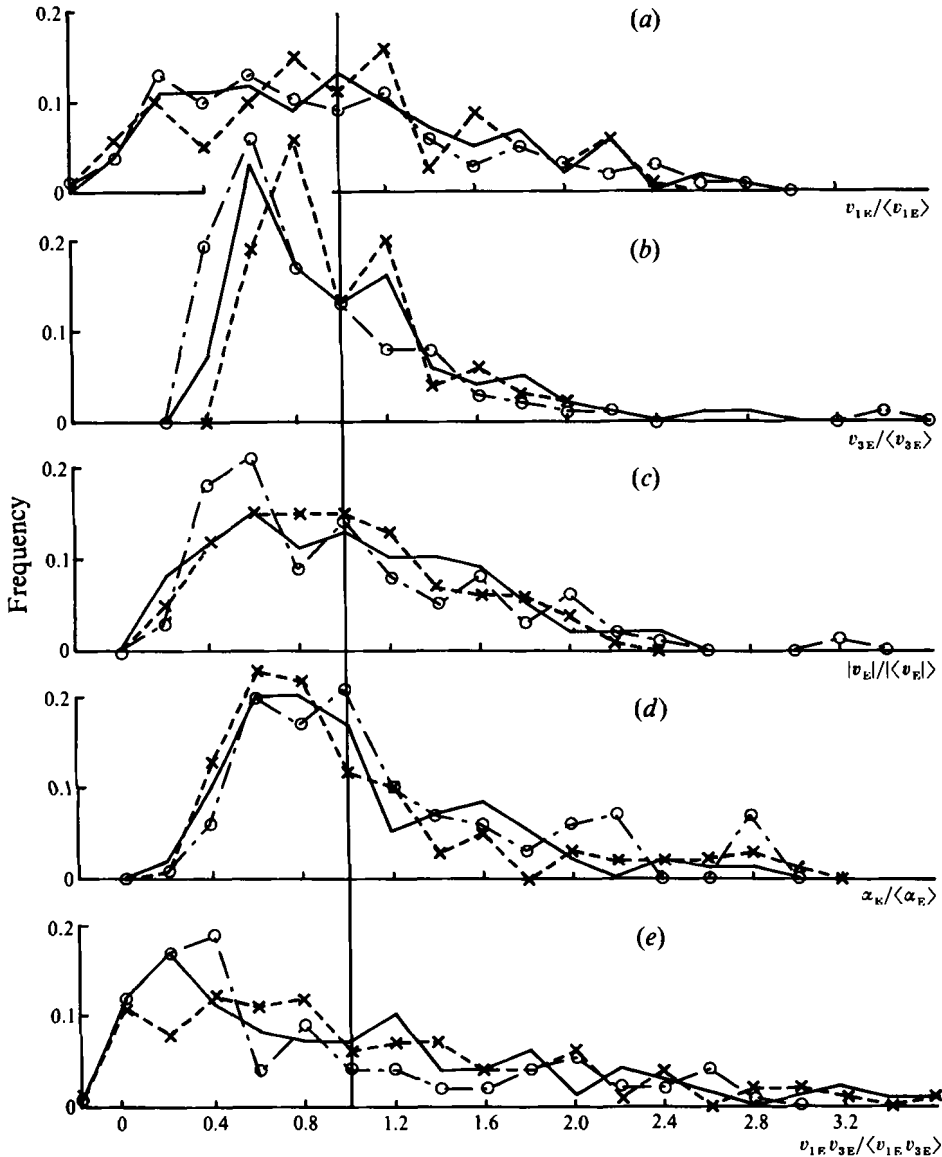


FIGURE 6. Frequency distribution of ejection velocity components and angle normalized on their mean values: (a) horizontal velocity  $v_{1E}$ , (b) vertical velocity  $v_{3E}$ , (c) speed  $|v|$ , (d) angle  $\alpha_E$ , (e) product of  $v_{1E}$  and  $v_{3E}$ ;  $\circ$ — $\circ$ , run 01; —, run 02;  $\times$ — $\times$ , run 03.

experimental results agree most closely with those of AM, whose experimental method closely resembles ours.

The vertical component of ejection velocity  $\langle v_{3E} \rangle$  is  $2.0u_*$  with a standard deviation of about  $1.0u_*$ . The correlation between the fluctuations in  $v_{3E}$  and in  $v_{1E}$  was also calculated, and found to be positive and about 0.5, which is certainly significant. Owen (1964) assumed that  $\langle v_{3E} \rangle$  was about equal to  $u_*$ . Sørensen (1985) has measured  $\langle v_E \rangle$  for a variety of sand particle sizes and has shown that it is maximum when  $D \approx 150 \mu\text{m}$ , decreasing by a factor of 2 when  $D = 300 \mu\text{m}$  and 4 when  $D = 900 \mu\text{m}$ .

AM found  $\langle v_{3E} \rangle / u_*$  was about 1.6. WS and WR did not record this value, but from

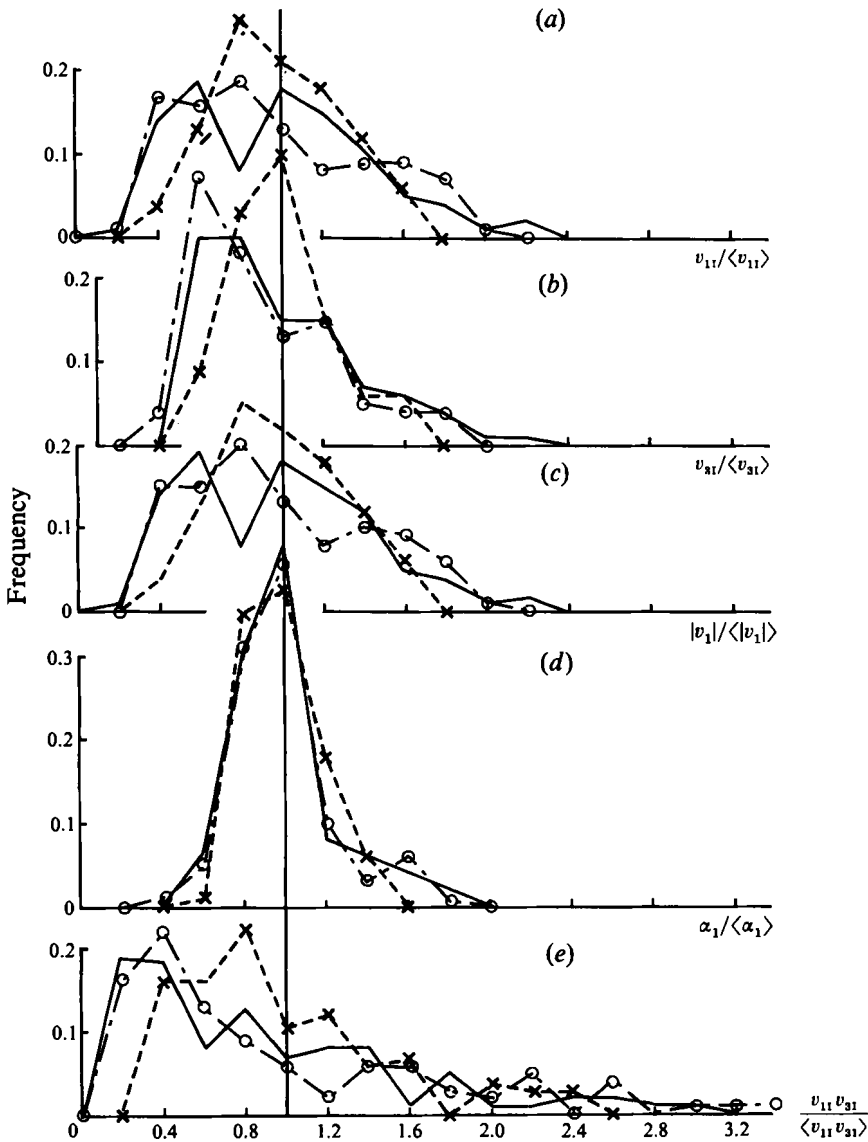


FIGURE 7. Frequency of impact velocity components and angle normalized on their mean values: (a) horizontal velocity  $v_{11}$ ; (b) vertical velocity  $v_{31}$ ; (c) speed  $|v_1|$ ; (d) angle  $\alpha_1$ ; (e) product of  $v_{11}$  and  $v_{31}$ ;  $\circ$ — $\cdot$ — $\cdot$ , run 01;  $\cdot$ — $\cdot$ — $\cdot$ , run 02;  $\times$ — $\cdot$ — $\cdot$ , run 03.

their data we can estimate the normalized vertical component of the mean ejection velocity  $(\langle v_E \rangle / u_*) \sin \langle \alpha_E \rangle$ . This is not the same as  $\langle v_{3E} \rangle / u_*$  since

$$\langle v_E \sin \alpha_E \rangle \neq \langle v_E \rangle \sin \langle \alpha_E \rangle.$$

For our data  $(\langle v_E \rangle / u_*) \sin \langle \alpha_E \rangle = 2.4$ . For AM, this ratio is 2.5, while for WS it is 1.4 and WR it is 2.1 to 3.2. So it appears that the measurements of the average vertical ejection velocity, normalized on  $u_*$ , are quite close for the three sets of data from WR, AM, the present work. There is obviously a discrepancy with that of WS.

The mean rise height  $\langle h \rangle$  of trajectories was measured by ourselves and AM. The standard deviation of  $h$  was approximately equal to the mean value for the  $118 \mu\text{m}$

particles and to 40% of  $\langle h \rangle$  for the 188  $\mu\text{m}$  ones. The results are normalized on the vertical kinetic energy per unit weight of the ejected particle,  $\langle v_{3E}^2 \rangle / 2g$ . (Note that the mean of the square of  $v_{3E}$ , i.e.  $\langle v_{3E}^2 \rangle$ , is about 25% greater than the square of the mean  $\langle v_{3E} \rangle^2$ .) We found that  $\langle h \rangle / (\langle v_{3E}^2 \rangle / 2g)$  varied between 0.59 and 0.43, which is close to the value measured by AM. Thus the effect of vertical drag on the particles is significant. Owen (1964) normalized  $\langle h \rangle$  on  $u_*$ , and predicted (with the assumption of  $v_{3E} = u_*$ ) that  $\langle h \rangle \approx 0.8u_*^2/g$ ; we find  $\langle h \rangle / (u_*^2/g)$  lies between 1.4 and 1.6.

The average lengths of the trajectories when normalized on the average trajectory height showed that  $\langle l \rangle / \langle h \rangle$  varied from 11 to 14, and when normalized on the square of the vertical velocity  $\langle l \rangle / (\langle v_{3E}^2 \rangle / 2g)$ , varied from 7.9 to 6.3. The standard deviation of  $l$  was about equal to  $\langle l \rangle$  for the small particles and about  $\frac{1}{2}\langle l \rangle$  for the larger 188  $\mu\text{m}$  particles. Maeno *et al.* (1985) measured  $\langle l \rangle$  for a range of snow particle sizes and over a range of wind speeds. They showed rather convincingly that  $l$  is indeed proportional to  $\bar{U}_0^2$ , over a range of  $\bar{U}_0$  from 4 to 9  $\text{m s}^{-1}$ , where  $\bar{U}_0$  is measured above the wind tunnel boundary layer. (However, Sørensen's 1985 indirect estimates of  $\langle l \rangle$  do not agree with the suggestion that  $\langle l \rangle$  is proportional to  $u_*^2$ .)

Using the value of  $\langle v_{3E}^2 \rangle$  from the experiments of AM leads to the value of  $\langle l \rangle / (\langle v_{3E}^2 \rangle / 2g)$  equal to about 7.0 given in table 1.

Our measurements of mean impact angles  $\langle \alpha_1 \rangle$  range from  $14^\circ$  for the larger to  $11^\circ$  for the smaller particles. This agrees closely with  $\langle \alpha_1 \rangle^*$ , which is derived from the ratio of the mean impact velocities ( $\langle v_{3I} \rangle / \langle v_{1I} \rangle$ ). The standard deviation is less than 25% of the mean. WS measured a higher value for their large particles – again probably because they missed out many of the low trajectories. AM found  $\langle \alpha_1 \rangle$  equal to  $11^\circ$ , and  $\langle \alpha_1 \rangle^*$  equal to  $13^\circ$ . Thus the discrepancies are small between different experiments presumably because this aspect of the particles' motion is less sensitive to initial conditions.

The average impact speed  $\langle v_I \rangle$  is found to be greater than the average ejection speed  $\langle v_E \rangle$  because the drag on the particle increases its speed. In our case the ratio  $\langle v_I \rangle / \langle v_E \rangle$  varies from 2 to 1.6. In WS it was 2.3, and in WR it was about 1.6. However, the vertical velocity of the particles is significantly reduced by anything up to 50%. There is good agreement between the means of all the experiments.

There is a positive correlation between the horizontal component of the impact velocity  $v_{1I}$  and the vertical ejection velocity  $v_{3E}$ ; also there is a strong (negative) correlation between  $v_{1I}$  and  $v_{3I}$ . Both these results are simply explained by the fact that larger ejection velocities lead to particles rising higher and gaining higher horizontal velocities, and on their return having larger impact velocities.

Frequency distributions of ejection and impact velocities, trajectory lengths and maximum rise heights are shown in figures 6, 7 and 8. Two features stand out: first, the distributions are strongly skewed; second, for a given quantity the distributions are similar in all the runs and hence independent of particle size for the two sizes in our experiments. The second feature suggests that if the mean ejection speed and angle can be specified, their distribution is also specified. We make use of this in our flux modelling. The broad similarity between these distributions and those measured by AM for snow particles with different density and different shear stress also suggests that these results should be generally applicable to any dry particles.

The skew distributions are found to approximate to log-normal forms for  $v_E$  and  $\alpha_E$  according to a  $\chi^2$ -test. The skew distribution is not surprising because a low-velocity cut-off corresponds to the threshold for particle movement. The mode or the most probable value of  $v_E$  is largely determined by the friction velocity  $u_*$ . The tail of the distribution is determined by those particles that are ejected with high velocities, which

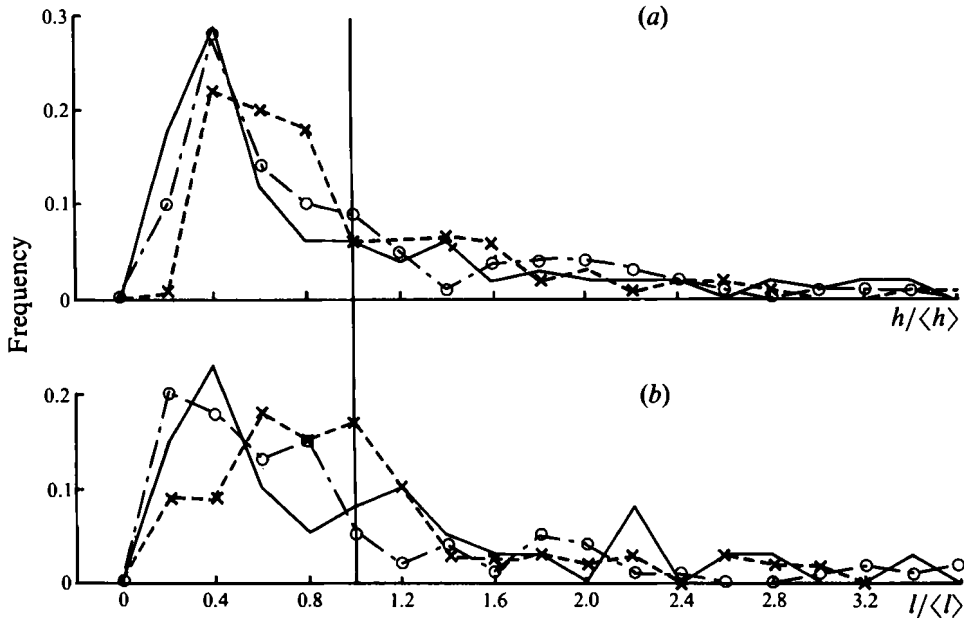


FIGURE 8. Frequency distributions of trajectory heights and lengths normalized on their mean values: (a) height  $h$ ; (b) length  $l$ ;  $\circ$ — — —  $\circ$ , run 01; — — —, run 02;  $\times$  — — —  $\times$ , run 03.

may be caused by unusual kinds of collision in the bed. Both these aspects of the distribution are affected by the particle size distribution and the nature of the surface, but not necessarily the particle density or shape, since  $v_E/u_*$  and  $\alpha_E$  have similar values for saltating sand and snow particles.

The probability distribution of the vertical component of ejection velocity,  $v_{3E}$ , shows a particularly sharp peak. Since the momentum of a particle either in the bed or impacting onto it is predominantly in the forward direction, there is a cutoff for the maximum possible vertical ejection velocity. The largest values of  $v_{3E}$  (and  $v_E$ ) may be associated with particularly energetic impacts.

The distributions of trajectory length  $l$  and maximum rise height  $h$  (figure 8) shows a much longer 'tail-off' than of the velocities, which might be expected because of their dependence on the squares of  $v_{1I}$  and  $v_{3E}$  respectively. The distribution of  $h$  broadly reflects that of  $v_{3E}$ .

Note how the impact angle distribution  $\alpha_I$  confirms that the impact angles generally lie within a few degrees of the mean value  $\langle \alpha_I \rangle$ .

The distribution of impact speeds  $v_I$  is more sharply peaked for the 118  $\mu\text{m}$  particles than for the 188  $\mu\text{m}$  ones. The computation of trajectories (see figure 10(b)) shows that, as the smaller particles descend, they respond more to the decrease in wind velocity near the bed. Hence their impact velocity is closer to the wind speed in the bottom few mm, whereas that of the larger particles is closer to that at the top of their trajectories. The upper limit of impact velocities is lower (in relation to the mean) than for ejection velocities: the latter display a large variation due to the stochastic nature of ejection, while the former are controlled by the wind speed, in particular the maximum value that a particle experiences, which is equal to about  $\bar{U}(h)$ .

Finally, we have observed from our photographs (as did WR) that occasionally particles are ejected backwards. The actual numbers are 2 out of 144 in run 01, 1 out of 120 in run 02 and 6 out of 113 in run 04. The reason could be either that such

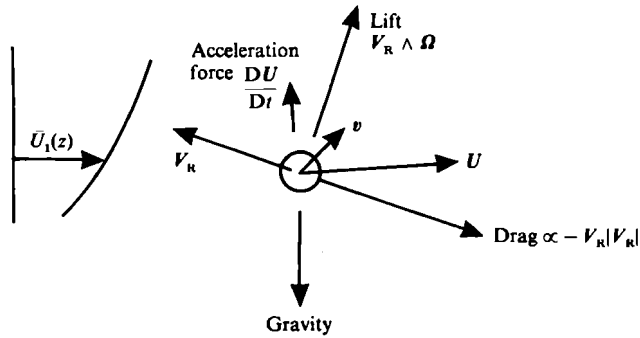


FIGURE 9. Forces acting on a spherical particle moving with velocity  $u$  through a flow with velocity  $U$ . The relative velocity is  $V_R = v - U$ .

particles are 'splashed up' by impacting particles, or that descending grains impact the upwind face of a local 'high spot' on the bed surface (even a larger grain). (This is consistent with the rather high standard deviation of  $\alpha_E$  which is 50% of its mean value.)

#### 4. Computation of trajectories

##### 4.1. Equations for particles in complex flows

In this section we analyse the nature and relative magnitudes of the forces acting on particles moving through a fluid with velocity  $v$ , see figure 9. In later sections we discuss the trajectories of particles.

Saffman (1965) derived an expression for the lift on a small sphere of radius  $a$  moving with relative velocity  $V_R = v - U$  in a steady shear flow  $\bar{U}_1(z)$  of a fluid with kinematic velocity  $\nu$  that is only valid if the Reynolds number of the particles  $Re_p = V_R a / \nu$  is small. But in saltation and even in suspension we usually find that  $50 \geq Re_p > 1$ . Rubinow & Keller (1961) obtained the lift force and torque on a sphere spinning with angular velocity  $\theta$  moving in a viscous unshered fluid, again for  $Re_p \ll 1$ . WS and White (1982) found that the spin, or Magnus effect, estimated from Rubinow & Keller's (1961) paper, was not negligible compared with drag in determining a sphere's airborne motion, and could lead to increases in the maximum height of about 20%. Despite the inapplicability of the theory (typically  $Re_p > 10$ ), it appears to give rise to more accurate trajectory simulations than drag alone.

Even in inviscid flow the vorticity  $\Omega = \nabla \times U$  of the flow must be considered (Auton, Hunt & Prud'homme 1988), which implies that a particle with high Reynolds number moving with a velocity  $V_R$  relative to the flow experiences an inviscid lift force (with the same sense as an aerofoil with circulation).

The inviscid lift force for a particle in a turbulent boundary layer is of the same order ( $\sim Lu_*^2/z$ ) as the low Reynolds number prediction for a particle spinning at an angular velocity of order  $u_*/z$  (which is reasonable for a particle on or close to the surface) (Owen 1964). This is consistent with the results of WS.

Even at a high value of  $Re_p$ , spin can also have an effect on the lift drag of a solid spherical particle. However, in our computations we ignore lift effects because our study of many photographs of particle trajectories showed that there was nothing unusual about the trajectories of spinning particles.

The effect of particle shape also needs to be considered (cf. Willetts 1983) if lift and inertial forces are considered.

Another effect on the particles is caused by the fluctuating vertical acceleration of the turbulence, which is of order  $u_*^2/z$ . This effect is comparable with the drag and lift forces within a distance above the bed of one or two grain sizes, but above this height its effect is negligible.

#### 4.2. Governing equations and trajectories in saltation

By neglecting lift and inertial forces, it follows that for a particle in saltation, when its height is above a few grain sizes ( $z \gg a$ ), the most significant forces acting on it are drag and gravity.

The equation for the forces on a spherical particle reduces to

$$\rho_p \frac{4}{3} \pi a^3 (dv/dt - g) = -\frac{1}{2} \rho_A C_D \pi a^2 V_R V_R, \quad (1)$$

where  $V_R = v - \bar{U}$ ,  $V_R = |V_R|$ ,  $\bar{U}$  is the mean velocity in the boundary layer,  $C_D$  is the drag coefficient and  $\rho_A$  the density of air. Thence the horizontal and vertical components of  $v$  are given by

$$\frac{dv_1}{dt} = -\frac{3C_D}{8a} \lambda V_{1R} V_R \quad (2)$$

and

$$\frac{dv_3}{dt} = -\left[ \frac{3}{8} \frac{C_D}{a} \lambda V_{3R} V_R + g \right], \quad (3)$$

where  $\lambda = \rho_A/\rho_p \approx \frac{1}{2} \times 10^{-3}$ . Given an initial velocity and the drag coefficient  $C_D$  (which varies with the Reynolds number of the particle), these two equations can be integrated forwards in time to simulate saltation trajectories. We have also used these equations to march backwards in time, in order to extrapolate measured trajectories back to their ejection point. The value of  $C_D$  as a function of  $Re_p$  is obtained from the expressions given by Morsi & Alexander (1972).

The first important point to note about the saltation is that (at high Reynolds number) a particle takes an inertial/drag time of order  $\tau_I (\approx a/\lambda U(h))$  to accelerate to the horizontal wind speed, but takes a gravitational travel time ( $\tau_g$ ) of order  $v_{3E}/g$  to rise to its maximum height, where  $v_{3E}$  is the velocity with which the particle leaves the surface (which was shown in §3 to be approximately equal to  $2u_*$ ). These two times are of the same order for a 100  $\mu\text{m}$  diameter sand particle when, as in our experiments,  $u_* \approx 0.2 \text{ m s}^{-1}$ . If  $\tau_I \gg \tau_g$ , the trajectories would be approximately symmetric. Since in practice  $\tau_I \approx \tau_g$ , the trajectories have the characteristic rapid rise and slow fall (figure 10*a*). As  $(u_*^2)/ag$  increases,  $\tau_I/\tau_g$  decreases. In figure 10(*b*) we have sketched graphs to show how the ratio of  $\tau_I/\tau_g$  affects particles' horizontal velocity. Note that for larger particles in saltation (where  $a \geq 100 \mu\text{m}$ )  $v_1$  increases throughout the trajectory, while for smaller particles it decreases on the descending path because they can respond faster to the lower mean wind speed.†

The second important point to note about saltation is that the Reynolds number of the particles  $Re_p$  is usually large enough for the drag to be approximately proportional to the square of the relative velocity and to be in the direction of the relative velocity  $V_R$ . (A slightly lower power like  $\frac{3}{2}$  is more accurate but the following argument is unaffected.) Then since the speed  $|v|$  ( $\approx 4u_*$  initially) is small in comparison with the

† Owen's (1964) analysis of saltation drew a similar distinction between a relaxation time (equivalent to our inertia time) and a trajectory time. But he did not emphasize the importance of the nonlinear drag law. However, our numerical factor for the mean value of  $h$  is within 30% of his value.

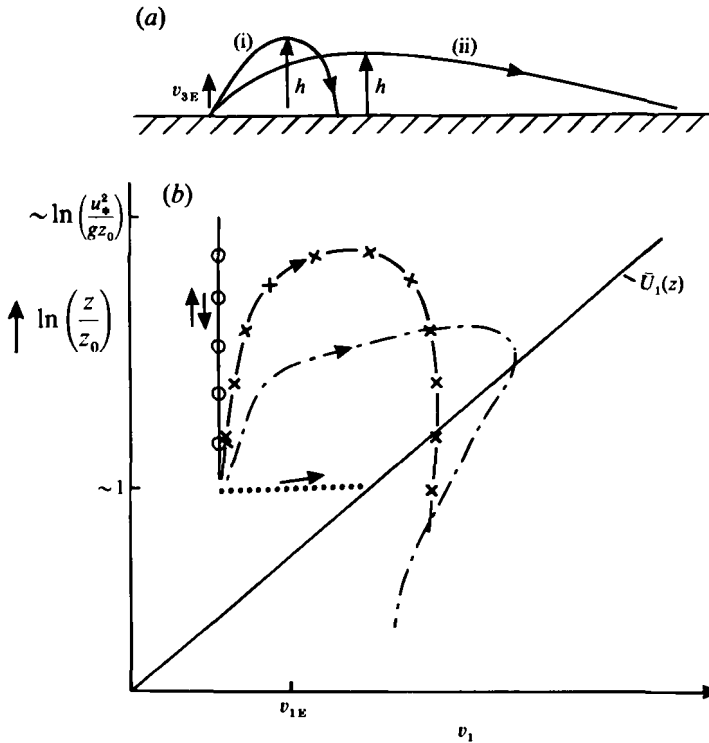


FIGURE 10. (a) Trajectories for two particles with the same vertical ejection velocity  $v_{3E}$ . (i)  $\tau_1 \gg \tau_g$ : gravitational force large compared with drag force;  $h \approx v_{3E}^2/2g$ . (ii)  $\tau_1 \leq \tau_g$ : gravitational force comparable with drag force;  $h < v_{3E}^2/2g$ . (b) Horizontal velocity component of particles along saltation trajectories with the same ejection velocity  $v_{1E}$ .  $\bar{U}_1(z)$  is the mean velocity profile: --O--, very heavy particles ( $\tau_1 \gg \tau_g$ ); --x--, heavy ( $\sim 200 \mu\text{m}$ ) ( $\tau_1 \sim \tau_g$ ); -.-.-, lighter ( $\tau_1 < \tau_g$ ); ....., very light particles.

mean wind speed  $\bar{U}_1(h)$  at the height  $h$  of saltation, the vertical drag is proportional to  $v_{3E}^2$ . With a low-Reynolds-number linear drag law the crosswind would have no effect on the vertical drag. Thus the ratio of the gravitational acceleration to the drag acceleration is  $ag/(\lambda \bar{U}_1 v_{3E})$  which is of the same order as  $\tau_1/\tau_g$ . So whenever  $\tau_1$  is less than  $\tau_g$ , and the parabolic trajectories are elongated, the vertical drag is significant (see figure 11 a). Typically for  $100 \mu\text{m}$  diameter sand particles it reduces  $h$  by about a factor of 2, and by much more as the particle size decreases. Of course the trajectory of the particle is also affected by the magnitude of the horizontal component of the ejection velocity  $v_{1E}$ . In figure 11 (b) we present computations showing how  $a$  and  $v_{1E}$  affect the ratio  $h/(v_{3E}^2/2g)$ .

The computations for a typical trajectory are given in table 1 for a  $200 \mu\text{m}$  diameter particle. Although a rather high value of ejection angle ( $45^\circ$ ) is taken, the results lie well within one standard deviation of the measured trajectories; in particular the impact angle  $\alpha_1$  is  $9^\circ$  compared with the measured values of  $11^\circ$ – $14^\circ$ , and the trajectory length  $l/(v_{3E}^2/2g)$  is 8.8 compared with the measurements of 6.3–7.0. Both of these differences may be caused by the actual velocity profile being slower near the surface than is assumed in this model calculation, where the log law profile extends to ground level.

The height of the trajectory  $h$  is normalized on  $v_{3E}^2$ : this agrees well with our measurements and those of AM and confirms the estimates of drag. In their paper AM



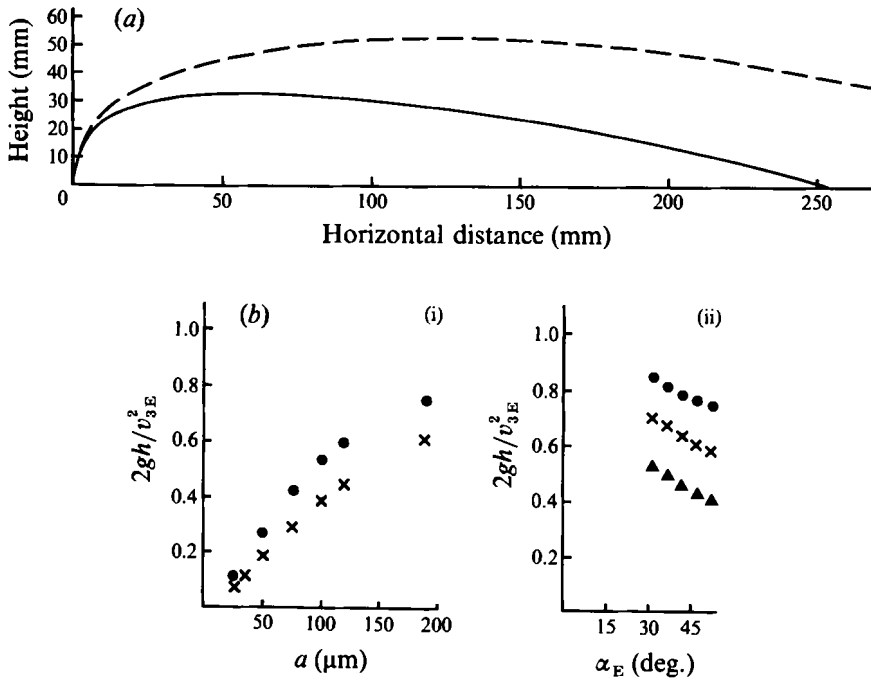


FIGURE 11. Computation of trajectories to show the effects of the vertical drag force. (a) Simulating trajectories for 188  $\mu\text{m}$  diameter particles with (—) and without (---) the component of drag in the vertical direction (largely caused by the mean horizontal wind!), at  $u_* = 0.20 \text{ m s}^{-1}$ ,  $z_0 = 0.07 \text{ mm}$ ;  $v_{1E} = 0$ ,  $v_{3E} = 1 \text{ m s}^{-1}$ . (b) Variation of maximum rise height of sand particles in saltation with (i) particle diameter; (ii) ejection angle ( $\alpha_E$ ). (i) ●,  $u_* = 0.2 \text{ m s}^{-1}$ ,  $v_{1E} = v_{3E} = 0.7 \text{ m s}^{-1}$ ; ×,  $u_* = 0.4 \text{ m s}^{-1}$ ,  $v_{1E} = v_{3E} = 1.0 \text{ m s}^{-1}$ . (ii) ●, 188  $\mu\text{m}$ ; ×, 118  $\mu\text{m}$ ; ▲, 75  $\mu\text{m}$ ;  $u_* = 0.2 \text{ m s}^{-1}$ ,  $v_E = 1.0 \text{ m s}^{-1}$ .

emphasized their finding that  $h$  was only about 60% of the height the particle would rise to in still air. They ascribed this effect to a 'negative lift' associated with some unidentified mechanism. The explanation is, as we have seen, quite simply that with a nonlinear drag law the large crosswind increases drag perpendicular to the wind. (Anyone cycling in a crosswind knows this effect only too well.)

Note that WS used their calculations of trajectories and an empirical correlation between the average impact and ejection velocities and angles to predict how  $v_1$  and  $v_3$  would change with the diameter of saltating particles. They predicted that both  $\alpha_E$  and  $v_1$  should increase with particle size, whereas WR found that  $\alpha_1$  and  $\alpha_E$  decreased! So more remains to be done to understand the effect of particle size on these statistics.

#### 4.3. Computing flux profiles from an ensemble of trajectories

As already explained, our measurements of the ejection velocity of saltating particles were used to provide the initial velocities for our trajectory computations. These data enabled us to calculate profiles of sand fluxes and concentrations over the flat sand bed corresponding to our experimental situation. These calculations were performed for grains in one size range only (mean diameter 188  $\mu\text{m}$ ), and for various wind speeds. The trajectories of an ensemble of particles are simulated, and statistics gathered of fluxes and concentration downwind.

Our method is to compute the trajectories of a large ensemble of particles whose

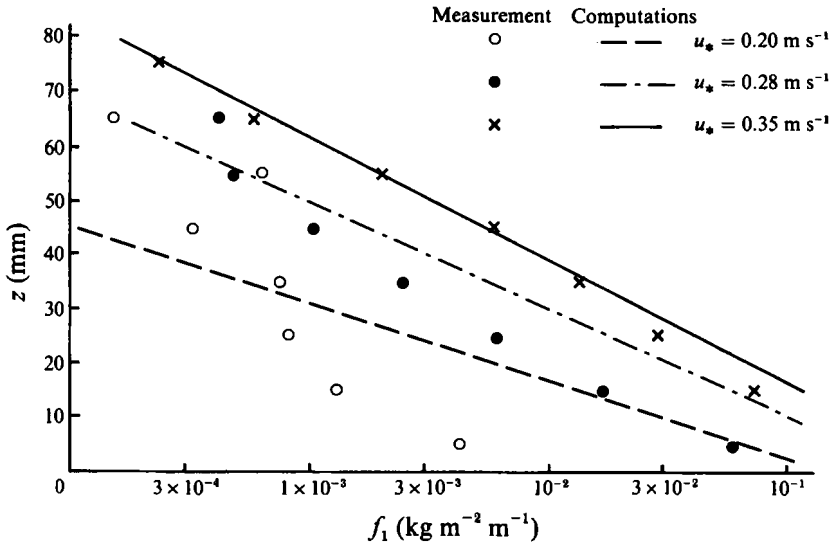


FIGURE 12. Simulated and measured horizontal fluxes  $f_1$  of sand grains above a flat horizontal sand bed. Grain diameter = 188  $\mu\text{m}$ .

initial horizontal and vertical velocities are chosen using a two-dimensional joint-normal random number distributions; initial positions along the bed and times are also chosen randomly. The number of particles passing a given point at a given height per unit time is counted to obtain fluxes, i.e. the computer model is an analogue of wind-tunnel and field experiments in which a series of traps are placed at the downwind end of a flat sand bed. Concentrations are similarly calculated by counting the number of particles in a given region of space at certain times.

Vertical profiles of horizontal flux normalized on an assumed upwind surface flux for 188  $\mu\text{m}$  sand grains are shown in figure 12, and compared with profiles measured in the wind tunnel at Warren Spring Laboratory. Our simulations do not agree well with the measurements for the case when  $u_* = 0.20 \text{ m s}^{-1}$ , which is close to threshold. At this wind speed the saltation is not fully developed, which may explain the disparity between measurements and simulations. However, the computations and experiments for higher wind speeds, when  $u_* = 0.28$  and  $0.35 \text{ m s}^{-1}$ , agree well with each other. The computed profiles clearly agree with the observed exponential decay with height: this form of profile has been found also by other workers, e.g. White (1982); Rasmussen *et al.* (1985), Gerety (1985), Williams (1964), Sørensen (1985) and White & Mounla (1991). Gerety also observes that the exponential profile is not observed at wind speeds very close to threshold.

The profiles of our computed fluxes and the measurements at Warren Spring Laboratory can be approximated by the relation

$$f_1(z)/f_{3E} \approx \alpha_c \exp(-\lambda_c z(u_*^2/g)), \quad (4a)$$

or by 
$$f_1(z) \approx f_1(0) \exp(-\lambda_m z/(u_*^2/g)), \quad (4b)$$

where  $\alpha_c$ ,  $\lambda_c$  and  $\lambda_m$  are dimensionless parameters and  $f_1(0)$  is the flux at the surface, obtained by extrapolation. Note that  $(u_*^2/g)$  is the approximate vertical scaling height

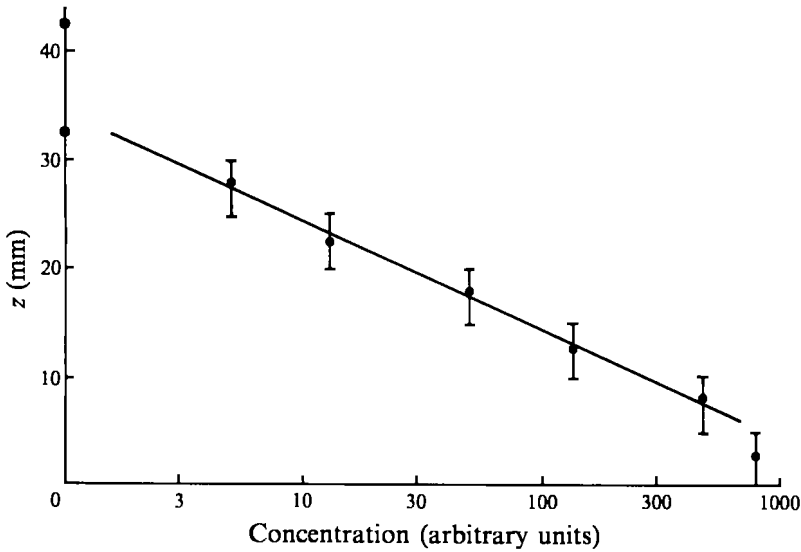


FIGURE 13. Simulated concentration profiles for 188  $\mu\text{m}$  sand grains over a flat bed.  $u_* = 0.2 \text{ m s}^{-1}$ ,  $z_0 = 0.07 \text{ mm}$ . Mean ejection speed  $v_E = 0.76 \text{ m s}^{-1}$ . Mean ejection angles  $\langle \alpha_E \rangle = 41^\circ$ . 'Error-bars' are height range over which each value of concentration is computed.

for the distribution. Evaluating the parameters from the computed and measured profiles shown in figure 13 gives the following results

| $u_*$<br>( $\text{m s}^{-1}$ ) | $\alpha_c$ | $\lambda_c$ | $f_1(0)$<br>( $\text{kg m}^{-2} \text{ s}^{-1}$ ) | $\lambda_m$ |
|--------------------------------|------------|-------------|---|-------------|
| 0.35                           | 57         | 1.2         | 0.59  | 1.2         |
| 0.28                           | 37         | 0.9         | 0.35  | 0.7         |

From the profiles measured at the Hanstholm experiment described by Rasmussen *et al.* (1985), we calculate a value of  $\lambda_m = 0.18$  for  $u_* = 0.63 \text{ m s}^{-1}$  (Run 2). (There does not yet seem to be any reliable way of relating wind-tunnel data to field measurements of  $\alpha$  and  $\lambda$ .)

We have to conclude that the vertical scale determining the exponential decay of  $f_1(z)$  has not been established as being proportional to  $u_*^2/g$ . A more recent investigation also shows a similar magnitude or variation of  $\alpha_c$  and  $\lambda$  (White & Maunla 1991).

The vertical profile (as opposed to flux) of concentration  $C(z)$  for given vertical flux  $\langle f_{3E} \rangle$  for  $u_* = 0.2 \text{ m s}^{-1}$  is shown in figure 14: this also decays exponentially with height.

#### 4.4. Computing 'effective' velocities of the particles

The 'effective' velocity  $\langle v_1 \rangle$  is the mean horizontal velocity of all (ascending and descending) particles between certain heights;  $\langle v_1 \rangle = f_1/C$ . A typical profile of  $\langle v_1 \rangle$  derived from a simulation is shown in figure 14(a). Close to the ground  $\langle v_1 \rangle$  is less than half  $\bar{U}_1$ ; but at the top of their trajectories  $\langle v_1 \rangle$  exceeds 90% of the mean velocity  $\bar{U}_1$ .

In figure 14(b) this graph has been scaled in more general coordinates as  $\langle v_1 \rangle / \langle v_1 \rangle (z = \langle h \rangle)$  (i.e. the mean particle velocity normalized on its value of  $z = \langle h \rangle$ ), against  $\ln(z/\langle h \rangle)$ , where  $\langle h \rangle$  is the mean trajectory height obtained from computations shown on figure 14(a). This enables us to compare this prediction with actual grain

velocity measurements by Greeley *et al.* (1983) for 400  $\mu\text{m}$  quartz particles in a wind tunnel ( $u_* = 0.55 \text{ m s}^{-1}$ ) and 300  $\mu\text{m}$  (median size) sand over a beach at Waddell Creek State Park, California. (We estimated the value of  $u_*$  as  $0.26 \text{ m s}^{-1}$  for this case from the measured value of  $6 \text{ m s}^{-1}$  at 1 m above the surface.) Their two curves showed quite different slopes, but we can see the explanation. Most of the latter measurements were taken where  $z \geq \langle h \rangle$  leading to a greater slope than in the former case where  $z \leq \langle h \rangle$ . The approximate agreement with model computations is rather remarkable given that  $\langle v_1 \rangle$  depends on the probability distribution of the velocity with which particles are emitted from the surface.

The fact that these profiles of  $f_1(z)$  and  $\langle v_1(z) \rangle$  are similar in a number of different flows suggests some degree of generality of these probability distributions. The graphs in figure 14(b) can be used as a basis for estimating concentration profiles  $C(z)$  from flux profiles  $f_1(z)$  or vice versa.

#### 4.5. Some speculations about fluxes and particle motions

By integrating the experimental curve for the vertical profiles of horizontal flux  $f_1(z)$ , the total horizontal flux per unit span  $F_1$  can be calculated. As Bagnold (1941) and many subsequent investigators found, and we confirmed in a number of tests (Barrett & Upton 1988)

$$F_1 \propto \rho_A u_*^3 / g, \quad (5a)$$

where  $\rho_A$  is the air density. For sand the constant of proportionality has been determined. Since  $F_1$  is zero for  $u_* < u_{*T}$ , the usual form of (5a) is

$$F_1 = (K_{sa} \rho_A / g) (D / D_0)^{1/2} [u_* - u_{*T}]^3, \quad (5b)$$

where  $K_{sa} \approx 0.6 \pm 0.3$  and  $D_0 \approx 250 \mu\text{m}$ . (In our experiment  $K_{sa} \approx 1.0$  and  $0.7$  at  $u_* = 0.35$  and  $0.28 \text{ m s}^{-1}$ .)

The flux  $F_1$  can in principle be computed from all the trajectories and from the vertical flux per unit area of particles leaving the surface,  $f_{3E}$ . Using the simulations and measurements reported in §4.3 we can now explore this relationship. If the probability that the trajectories of small samples of particles taken at random with equal vertical mass flux per unit area having a length between  $x$  and  $x + dx$  is  $p_l(x) dx$ , the probability that the particles have a trajectory greater than  $x$  is  $\int_x^\infty p_l(x') dx'$ . If the vertical flux of those particles per unit area is  $f_{3E}(x)$ , then the flux  $\delta F_1^{(x)}$  of particles that leave the surface between  $x$  and  $x + dx$  is  $f_{3E}(x) dx$  multiplied by the probability that they have a trajectory greater than  $x$ , i.e.

$$\delta F_1(x) = f_{3E}(x) \left( \int_x^\infty p_l(x') dx' \right) dx. \quad (6a)$$

By integrating this over all values of  $x_1$ , we obtain the total horizontal flux per unit span

$$F_1 = \int_0^\infty f_{3E}(x) \left( \int_x^\infty p_l(x') dx' \right) dx. \quad (6b)$$

Since  $\int_0^\infty x p_l(x) dx = \langle l \rangle$ , where  $\langle l \rangle$  is the average length of the trajectories and if  $f_{3E}(x)$  is a constant defined as  $\langle f_{3E} \rangle$ , then integrating (6b) by parts leads to

$$F_1 \approx \langle f_{3E} \rangle \langle l \rangle. \quad (6c)$$

(The result (6c), but not (6b), was first suggested by Jensen & Sørensen 1986; but their interpretation of (6b) in terms of the measurements differs from ours.)

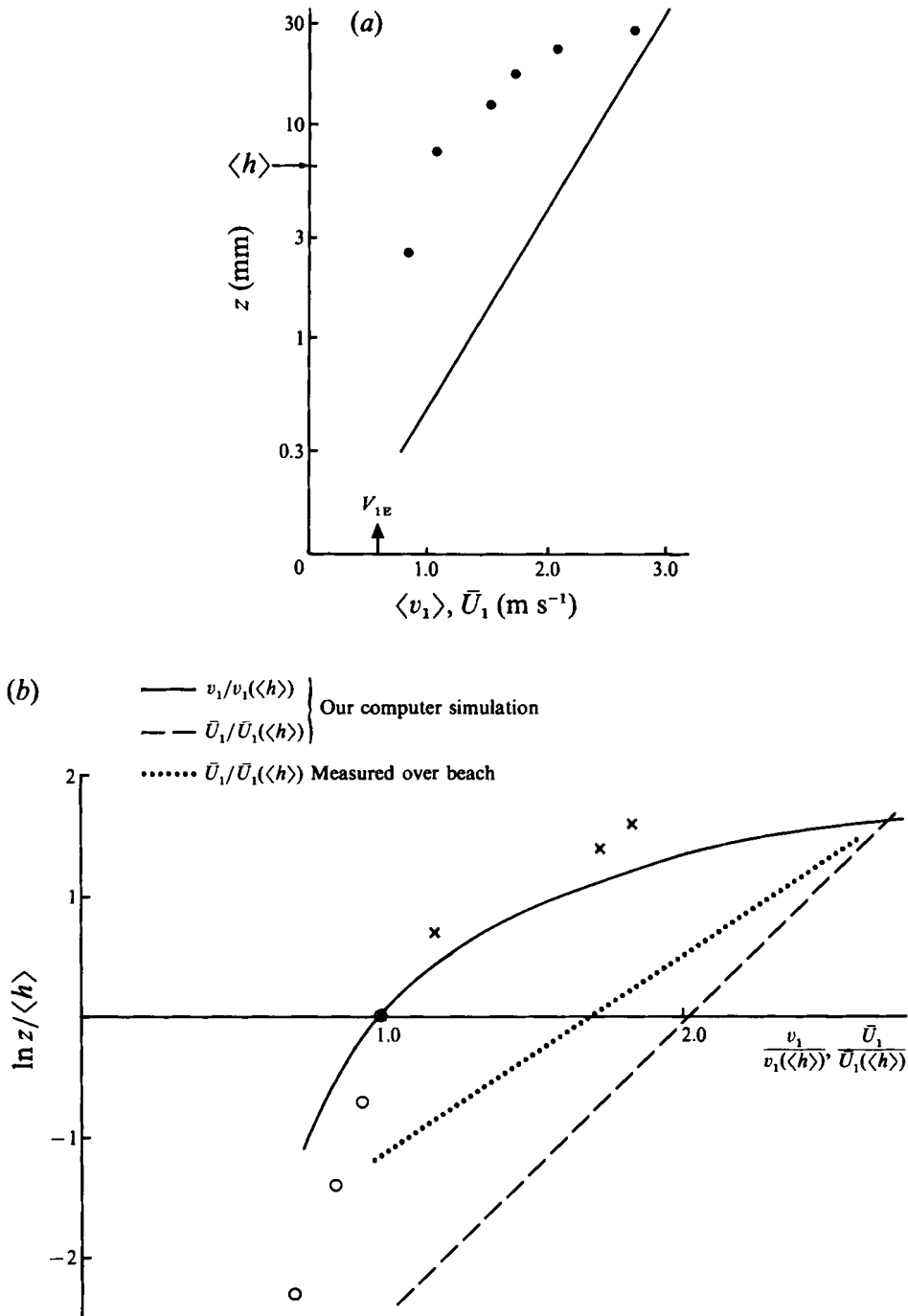


FIGURE 14. Computed values of the effective or mean velocity  $\langle v_1 \rangle = \text{flux}/\text{concentration}$  of sand particles compared with the mean wind velocity  $\bar{U}_1$ . (a) For a specific simulation, the results are plotted in dimensional terms. The conditions are as in figure 13:  $\bullet$ ,  $\langle v_1 \rangle$ ; —,  $\bar{U}_1$ . (b) Comparisons for the measured mean velocities  $\langle v_1 \rangle$  of 400  $\mu\text{m}$  quartz particles in a wind tunnel  $\odot$ , and 300  $\mu\text{m}$  sand particles over a beach  $\otimes$ . Also shown are simulations of  $\langle v_1 \rangle$  for a particular wind profile  $U_1$ . Note the plotting of various experiments and simulations by normalizing in terms of mean height of the trajectories,  $\langle h \rangle$  and the mean particle velocity at  $\langle h \rangle$ ,  $\langle v_1 \rangle$  ( $z = \langle h \rangle$ ), and the mean wind speed at  $\langle h \rangle$ ,  $U_1(\langle h \rangle)$  respectively.

Using the computations and measurements of trajectories given in table 1, which show that

$$\langle l \rangle \approx 16u_*^2/g, \quad (7)$$

the prediction of (6b) implies that the integrated horizontal flux is related to the average vertical flux by

$$F_1/\langle f_{3E} \rangle \approx 16u_*^2/g. \quad (8a)$$

This prediction can be compared with the simulations shown in figure 13. In the simulations the local height-dependent flux  $f_1(z)$  is computed as the ratio  $f_1(z)/\langle f_{3E} \rangle$  and thence  $F_1/\langle f_{3E} \rangle$  is computed.

For the highest-velocity case of  $u_* = 0.35 \text{ m s}^{-1}$ , it was found that

$$F_1/\langle f_{3E} \rangle \approx \alpha_c u_*^2/\lambda_c g \approx 47u_*^2/g. \quad (8b)$$

Clearly the two results in (8a) and (8b) are inconsistent. The most likely reason is that the vertical flux  $f_{3E}$  is highly intermittent and probably strongly correlated with the longest trajectories ( $l$ ). This would mean that  $F_1$  is generally significantly greater than the product  $\langle f_{3E} \rangle \langle l \rangle$ . In the sample chosen for computing,  $l$  was based on the number of particles in a certain layer which were leaving the surface. It was not based on samples of equal flux. Our procedure would lower  $\langle l \rangle$ .

This has implications for trajectories and for estimations of the drag on the air flow caused by the particle trajectories (such as those of Bagnold 1941, chap. 4 or Owen 1964).

The other implications of (4), (5) and (6) is that

$$\langle f_{3E} \rangle \propto \rho_A u_*, \quad (9)$$

with the constant of proportionality being about  $\frac{0.6}{47}(D/D_0)^{\frac{1}{2}}$ , i.e. about  $10^{-2}$ .

Our measurements and those of Sørensen (1985) agree that

$$\langle f_{3E} \rangle \approx 10^{-2} \text{ kg m}^{-2} \text{ s}^{-1} \quad (10)$$

for sand particles when  $u_* \approx 0.34 \text{ m s}^{-1}$ . But Sørensen (1985) does not agree that  $\langle f_{3E} \rangle$  is proportional to  $u_*$ . This estimate for  $\langle f_{3E} \rangle$  implies that there are about a hundred (200  $\mu\text{m}$  diameter) particles leaving per  $\text{cm}^2$  per s (i.e. about 1 in 100 in the surface consisting of 100  $\mu\text{m}$  particles).

This estimation of  $\langle f_{3E} \rangle$  is necessary to develop simulations of trajectories of particles near the sharp crest of a stockpile or of a sand dune as they are carried into the separated flow region (Nalpanis & Hunt 1986).

From the estimation of  $\langle f_{3E} \rangle$ , based on our simulation and the measurement of flux, it is possible to estimate the mean concentration  $C$  per unit volume, by noting that

$$f_1(z) = \langle f_{3E} \rangle f_1(z)/\langle f_{3E} \rangle \approx \langle v_1 \rangle \rho_p C. \quad (11)$$

Since  $\langle v_1 \rangle \propto u_*$ ,  $\langle f_{3E} \rangle \propto u_*$ , and  $f_1/\langle f_{3E} \rangle$  is approximately independent of  $u_*$  (for given  $z/(u_*^2/g)$ ), it follows that  $C$  is also approximately independent of  $u_*$  for given  $z/(u_*^2/g)$ . It follows that at a typical saltation height of  $z \approx u_*^2/g$ , the order of magnitude of  $C$  is about  $0.2 \times 10^{-4}$  for sand particles, for the wind speeds considered here. The average density of particles compared to that of air is only about 0.05. Presumably this is why there is only a small effect on the mean wind profile over the limited fetch of the experiments. Bagnold's (1941) experiments and others show that the saltating particles do affect the wind profile over a longer fetch even at values of  $u_*$  as low as  $0.35 \text{ m s}^{-1}$ .

## 5. Conclusions

In this paper we have presented new measurements of the statistics of the velocities of ejection and impact of sand particles saltating in a turbulent air flow over a sand bed. These measurements support previous suggestions that the mean ejection velocity is proportional to the friction velocity and does not vary much with the grain size. The actual values agree with other measurements by Willetts & Rice (1985) and Araoka & Maeno (1981), but differ from those of White & Schulz (1977). We have also measured the vertical profiles of the horizontal flux of saltating particles and found, as have other investigators, that the flux decreases exponentially with distance above the surface, once the wind speed is more than about 50% above threshold value.

Trajectories have also been computed, first to estimate by extrapolation the ejection and impact velocities of the measured trajectories, and second to calculate the flux profiles. We have shown that the nonlinear, non-Stokesian drag acting on the particles leads to a significant vertical drag which reduces by about 40% the height to which particles rise. We have assumed that the probability distribution of ejection velocities and the ratio of ejection to friction velocity do not vary greatly with wind speed above the threshold, which implies that the flux profile should not change as the wind speed varies. In fact the flux profile did change, and become closer to the computed form at the higher wind speed (again as White & Mounla 1991 have confirmed). Both the assumptions and its implications need further examination. A relation has been proposed between the total horizontal flux, theoretical flux density and the probability distribution of the trajectory.

Recently the interaction between the impacting particles and the particles in the bed have become better understood, through experiments and computer simulation of the mechanics of a solid body hitting a bed of other solid bodies (see Anderson *et al.* 1991). This should lead to models for the variation in the statistics of ejection with wind speed. The other main problem in saltation is the effect of the particles on the flow. Recent studies of simpler two-phase flows where particles control turbulent flows (Ghosh, Phillips & Perkins 1991) may help improve understanding of how air flow in the saltation layer is affected by particles being ejected into the flow with such different speeds.

P. N. and J. C. R. H. are grateful for support of this work from the Department of Trade and Industry (Warren Spring Laboratory). They are also grateful for the help with the wind-tunnel experiments at Warren Spring Laboratory from S. Upton.

We benefited from useful conversations with the late Professor P. R. Owen and with the participants at the conference at Aarhus in 1985 organized by Professor O. Barndorff-Nielsen. The referees made many useful suggestions for improving the paper.

## REFERENCES

- ABSIL, F. G. J. & BEUGELING, G. L. H. 1984 The entrainment of small particles by a turbulent spot. In *Atmospheric Dispersion of Heavy Gases and Small Particles – IUTAM Symp. Delft, 1983*, pp. 211–219. Springer.
- ANDERSON, R. S. 1987 A theoretical model for aeolian impact ripples. *Sedimentol.* **34**, 943–956.
- ANDERSON, R. S. & HAFF, P. K. 1991 Wind modification and bed response during saltation of sand in air. *Acta Mech. (Suppl.)* **1**, 21–52.
- ANDERSON, R. S., SORENSEN, M. & WILLETTS, B. B. 1991 A review of recent progress in our understanding of aeolian sediment transport. *Acta Mech. (Suppl.)* **1**, 1–19.

- ARAOKA, K. & MAENO, N. 1981 Dynamical behaviour of snow particles in the saltation layer. In *Proc. 3rd Symp. on Polar Met. & Glaciology. Mem. Natl Inst. Polar Res., Tokyo*, no. 19, pp. 253–263 (referred to herein as AM).
- AUTON, T. J., HUNT, J. C. R. & PRUD'HOMME, M. 1988 The force exerted on a body in inviscid unsteady non-uniform rotational flow. *J. Fluid Mech.* **197**, 241–257.
- BAGNOLD, R. A. 1941 *The Physics of Blown Sand and Desert Dunes*. Methuen.
- BARNDORFF-NIELSEN, O. E. 1985 (Ed.) *Proc. Intl Workshop on the Physics of Blown Sand, Department Theor. Stat., University of Aarhus, Denmark*.
- BARRETT, C. F. & UPTON, S. L. 1988 Erodibility of stockpiled materials – a windtunnel study. *Warren Spring Laboratory, Stevenage, UK Rep.* LR 656 (PA).
- COUNIHAN, J. 1969 An improved method of simulating an atmospheric boundary layer in a wind tunnel. *Atmos. Environ.* **3**, 197–214.
- FLETCHER, R. 1976 The incipient motion of granular materials. *J. Phys. D: Appl. Phys.* **9**, 2471–2478.
- GERETY, K. M. 1985 Problems and determination of  $u_*$  from wind-velocity profiles measured in experiments with saltation. In *Proc. Intl Workshop on the Physics of Blown Sand* (ed. O. E. Barndorff-Nielsen), vol. 2, pp. 271–300. University of Aarhus, Denmark.
- GHOSH, S., PHILLIPS, J. C. & PERKINS, R. J. 1991 Modelling the flow in droplet driven sprays. In *Advances in Turbulence 3* (ed. A. V. Johansson & P. H. Alfredsson), pp. 93–100. Springer.
- GILLETTE, D. A. & STOCKTON, P. H. 1986 Mass momentum and kinetic energy fluxes of saltating particles. In *Aeolian Geomorphology, Proc. 17th Ann. Binghamton Geomorphology Symp., Sept. 1986* (ed. W. G. Nickling), pp. 35–56. Allen and Unwin.
- GREELEY, R., WILLIAMS, S. H. & MARSHALL, J. R. 1983 Velocities of windblown particles in saltation: preliminary laboratory and field measurements. In *Eolian Sediments and Processes* (ed. M. E. Brookfield and T. S. Ahlbrandt). Elsevier.
- HUNT, J. C. R. & NALPANIS, P. 1985 Saltating and suspended particles over flat and sloping surfaces I. Modelling concepts. In *Proc. Intl Workshop on Physics of Blown Sand* (ed. O. E. Barndorff-Nielsen), vol. 1, pp. 9–36. *Mem.* 8. University of Aarhus, Denmark.
- IVERSON, J. D. & WHITE, B. R. 1982 Saltation threshold on Earth, Mars and Venus. *Sedimentol.* **28**, 111–119.
- JENSEN, J. L. & SØRENSEN, M. 1986 Estimation of some aeolian saltation transport parameters: a reanalysis of Williams' data. *Sedimentol.* **33**, 547–558.
- MAENO, N., ARAOKA, K., NISHIMURA, K. & KANEDA, Y. 1979 Physical aspects of the wind-snow interaction in blowing snow. *J. Fac. Sci., Hokkaido Univ.* VII **6**, 126–141.
- MORSI, S. A. & ALEXANDER, A. J. 1972 An investigation of particle trajectories in two-phase systems. *J. Fluid Mech.* **55**, 193–208.
- NALPANIS, P. 1985 Saltating and suspended particles over flat and sloping surfaces. II. Experiments and numerical simulations. In *Proc. Intl Workshop on Physics of Blown Sand* (ed. O. E. Barndorff-Nielsen), vol. 1, pp. 37–66. *Mem.* 8. University of Aarhus, Denmark.
- NALPANIS, P. & HUNT, J. C. R. 1986 Suspension, transport and deposition of dust from stockpiles. *Warren Spring Laboratory, Stevenage, England Rep.* CR 277(PA).
- OWEN, P. R. 1964 Saltation of uniform grains in air. *J. Fluid Mech.* **20**, 225–242.
- OWEN, P. R. & GILLETTE, D. A. 1985 Wind tunnel constraint on saltation. In *Proc. Intl Workshop on the Physics of Blown Sand* (ed. O. E. Barndorff-Nielsen), vol. 2, pp. 253–270. *Mem.* 8. University of Aarhus, Denmark.
- RASMUSSEN, K. R., SØRENSEN, M. & WILLETTS, B. B. 1985 Measurement of saltation and wind strength on beaches. In *Proc. Intl Workshop on the Physics of Blown Sand* (ed. O. E. Barndorff-Nielsen), vol. 2, pp. 301–325. *Mem.* 8. University of Aarhus, Denmark.
- RAUPACH, M. R. 1991 Saltation layers, vegetation canopies and roughness lengths. *Acta Mechanica* (Suppl) **1**, 83–96.
- RUBINOW, S. I. & KELLER, J. B. 1961 The transverse force on a spinning sphere moving in a viscous fluid. *J. Fluid Mech.* **11**, 447–459.
- SAFFMAN, P. G. 1965 The lift on a small sphere in a slow shear flow. *J. Fluid Mech.* **22**, 385–400.
- SØRENSEN, M. 1985 Estimation of some aeolian saltation transport parameters from transport rate



- profiles. In *Proc. Intl Workshop on the Physics of Blown Sand* (ed. O. E. Barndorff-Nielsen), vol. 1, pp. 141–190. *Mem. 8*. University of Aarhus, Denmark.
- WHITE, B. R. 1982 Two-phase measurements of saltating turbulent boundary layer flow. *Intl J. Multiphase Flow* **8**, pp. 459–473.
- WHITE, B. R. & MOUNLA, H. 1991 An experimental study of Froude number effect on wind-tunnel saltation. *Acta Mechanica* (Suppl.) **1**, 145–157.
- WHITE, B. R. & SCHULZ, J. C. 1977 Magnus effect in saltation. *J. Fluid Mech.* **81**, 497–512 (referred to herein as WS).
- WILLETTS, B. B. 1983 Transport by wind of granular materials of different grain shapes and densities. *Sedimentol.* **30**, 669–679.
- WILLETTS, B. B. & RICE, M. A. 1985 Intersaltation collisions. In *Proc. Intl Workshop on the Physics of Blown Sand* (ed. O. E. Barndorff-Nielsen), vol. 1, pp. 83–100. *Mem. 8*. University of Aarhus, Denmark (referred to herein as WR).
- WILLIAMS, G. 1964 Some aspects of the eolian saltation load. *Sedimentol.* **3**, 257–287.